Journal of Alloys and Compounds 509 (2011) 3108–3115

Contents lists available at ScienceDirect

Journal of Alloys and Compounds

journal homepage: www.elsevier.com/locate/jallcom

Sensing properties of sprayed antimony doped tin oxide thin films: Solution molarity

A.R. Babar[a], S.S. Shinde[a], A.V. Moholkar[b], C.H. Bhosale[a], J.H. Kim[c], K.Y. Rajpure[a,*]

[a] Electrochemical Materials Laboratory, Department of Physics, Shivaji University, Kolhapur 416 004, India
[b] Department of Physics, Gopal Krishna Gokhale College, Kolhapur 416 012, M.S., India
[c] Department of Materials Science and Engineering, Chonnam National University, 300 Yongbong-Dong, Buk-Gu, Gwangju 500-757, South Korea

ARTICLE INFO

Article history:
Received 14 October 2010
Received in revised form
26 November 2010
Accepted 2 December 2010
Available online 10 December 2010

Keywords:
Concentration
Structural
Optoelectronic properties
Photoluminescence
Gas sensor

ABSTRACT

Transparent conductive thin films of nanocrystalline Sb:SnO_2 have been deposited onto preheated glass substrates by using spray pyrolysis technique. The effect of the solution molarity on structural, morphological, optoelectronic properties of Sb:SnO_2 films has been investigated. XRD study reveals that films are polycrystalline with tetragonal crystal structure having average crystallite size about 20 nm. The compact and homogeneous grains are seen in FESEM images. The BEs of Sn $3d_{5/2}$ for all samples show the Sn^{4+} bonding state for SnO_2. The BEs of Sb $3d_{5/2}$ are in the range of 530.6–530.9 eV, indicating that all antimony detected is in a pentavalent state (Sb^{5+}). Transparency of films in the visible region decreases with increase in precursor concentration. Photoluminescence study shows the strong violet and weak orange emission. The sensing properties of the Sb:SnO_2 films for acetone, ethanol and LPG with operating temperature and gas concentration have been investigated.

1. Introduction

The metal oxide semiconductor gas sensor is based on the conductivity change of the semiconductor material due to its interaction with gas. When gas molecules are adsorbed on the surface of a semiconductor, electron transfer occurs between the semiconductor and the adsorbates. If the electron affinity of the adsorbates is larger than the work function of the n-type semiconductor, the adsorbates accept electrons from the semiconductor. In the opposite case, the semiconductor accepts electrons from the adsorbates. This electron transfer continues until the Fermi level of the gas adsorbed semiconductor surface becomes equal to that of the bulk [1]. As a result of this electron transfer, a depletion or accumulation of charges occurs near the semiconductor surface. Then, the accompanying variation of surface potential barrier induces a change in the electrical conductivity or resistivity. Numerous metal oxide semiconductor materials were reported to be used as semiconductor gas sensors, such as ZnO, SnO_2, WO_3, TiO_2, Fe_2O_3, and In_2O_3. These candidates have microstructural defects, so free electrons originating from oxygen vacancies contribute to electronic conductivity [2]. The demands for accurate and dedicated sensors to provide precise process control and automation in manufacturing process, and also to monitor and control environmental pollutions, have accelerated the development of new sensing materials and sensors technology [3]. Most studies have focused on detecting the toxic and the flammable gases, present in the atmospheric composition in some environments, such as acetone, ethanol and LPG. It is believed that sensor sensitivity can be improved by the varying solution concentration or the increasing specific surface area of the sensitive materials. The materials will provide more surface sites available for oxygen to be adsorbed on them and to make contact with the surrounding gases [4]. The synthesis of ATO is of great technological and scientific interests owing to the use of these materials as transparent electrodes, heat mirrors, displays, electrochromic windows, catalysts, rechargeable Li batteries, and energy storage devices and has potential uses in photovoltaic and optoelectronic devices [5,6]. Other interesting features of ATO are their gas sensing properties. Several methods have been used to prepare antimony doped tin oxide thin films such as chemical vapour deposition (CVD) [7], sputtering [8], sol–gel [9], atomic layer epitaxy [10] and spray pyrolysis [11,12]. It has been shown that antimony doped tin oxide films with good electronic properties can be achieved by tuning precursor concentration in spray pyrolysis technique.

The carrier concentration and mobility can be controlled by monitoring substrate temperature and amount of antimony doping. Apart from the different preparative parameters like thickness, quantity of the spraying solution, starting material, dopant, nozzle–substrate distance and air flow rate, precursor concentration also plays an important role for obtaining the device quality properties of the Sb:SnO_2 thin films. The present manuscript

* Corresponding author. Tel.: +91 231 2609435; fax: +91 231 2691533.
E-mail address: rajpure@yahoo.com (K.Y. Rajpure).

0925-8388/$ – see front matter © 2010 Elsevier B.V. All rights reserved.
doi:10.1016/j.jallcom.2010.12.012

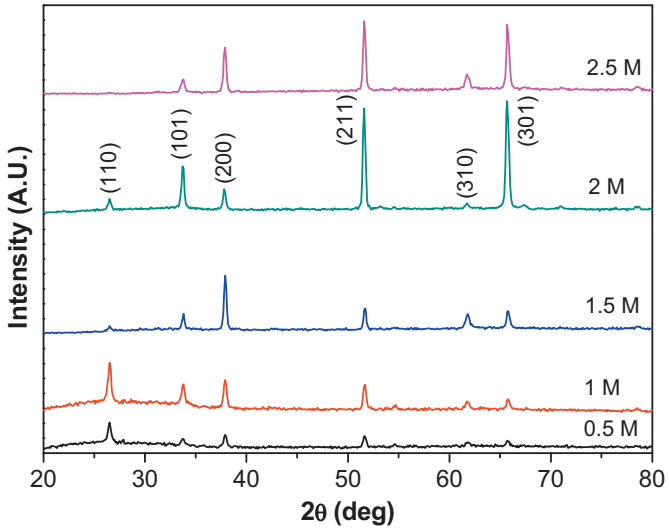

Fig. 1. X-ray diffraction patterns for the Sb:SnO_2 thin films deposited at various concentrations of $SnCl_4$ in solution.

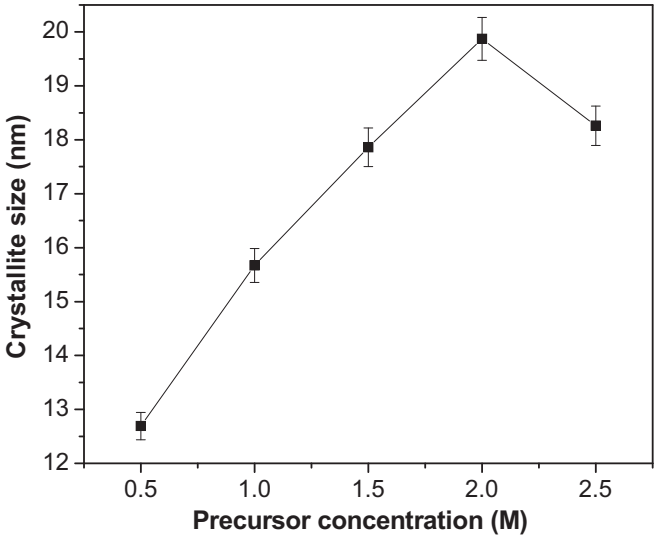

Fig. 2. Variation of average crystallite size of sprayed Sb:SnO_2 thin films for different concentrations of $SnCl_4$ in solution.

reports the effect of precursor concentration on the structural, morphological, optical and luminescent properties of spray-deposited Sb:SnO_2 thin films. The sensing characteristics of Sb:SnO_2 thin films for various gases such as acetone, ethanol and LPG were investigated.

2. Experimental

Stannic chloride (Thomas Baker), antimony trichloride (s.d. fine) and 2 propanol (solvent) were used in the present case. The glass substrates (75 mm × 25 mm × 1.2 mm) supplied by Blue Star, Mumbai were used. The solution flow rate (5 ml/min) was controlled by carrier gas (air) having pressure ~1.5 kg cm^{-2}. The amount of $SbCl_3$ and substrate temperature were kept fixed at 2 at% and 475 °C respectively, which have been found to be optimal for achieving good quality Sb:SnO_2 thin films. The quantity of the solvent 2 propanol (10 ml) was kept constant throughout the experiments. The concentration of $SnCl_4 \cdot 5H_2O$ in the spraying solution has been varied from 0.5 M to 2.5 M. We restricted to this limit of $SnCl_4$ concentration because at higher concentrations (>2.5 M), the solution becomes more viscous and small particles collect at the spray nozzle tip, which results in powdery films with high sheet resistance. The chromel–alumel thermocouple, connected to a temperature controller was used to record temperature of glass substrates. It has been observed that, when the metallic solution was sprayed onto hot substrates (at optimized substrate temperature), pyrolytically decomposed good quality Sb:SnO_2 thin films were formed. These films were then allowed to cool at room temperature and further used for structural, optical, and electrical characterization.

The structural properties were studied by a Powder X-ray diffractometer [Bruker D8 Advance, France] using Cu-kα radiation in the 2θ range of 20–80°. SAED analysis was carried out with a Philips CM-12 electron microscope (point resolution 2.8 Å). The morphology of the films was observed by field emission scanning electron microscopy (FESEM) (Model: JSM-6701F, Japan). X-ray photoelectron spectroscopic studies were carried out using the model PHI-5400 type X-ray photoelectron spectroscope (Physical Electronics PHI 5400, USA) with monochromatic Mg-K_α (1254 eV) radiation source. Optical absorption study was carried out in the wavelength range 300–1100 nm using double beam spectrophotometer (SHIMADZU UV-1700, Japan). The room temperature photoluminescence spectra of the films were recorded using a Perkin-Elmer luminescence spectrometer (Model: LS55, USA). All spectra were measured at room temperature with an Ar ion laser as a light source using an excitation wavelength of 325 nm. The sensing properties of Sb:SnO_2 thin films were studied in an indigenous gas sensor unit. For electrical measurements, silver paste contacts (1 mm) were made on the Sb:SnO_2 sample of area 1 cm^2. Gas concentration in the measurement chamber was monitored with calibrated gas flow meter.

3. Results and discussion

3.1. Structural analysis

Fig. 1 shows X-ray diffraction patterns of Sb:SnO_2 films prepared at typical substrate temperature of 475 °C grown on glass substrates with different solution molarities in spraying solution. The deposited films are polycrystalline having tetragonal crystal structure. The crystallinity of the films increases up to 2 M concentration and then decreases for higher concentration. The films deposited with lower solution concentrations (0.5 M and 1 M) show orientation along (1 1 0) plane, whereas film deposited at 1.5 M solution concentration shows orientation along (2 0 0) plane. While peak intensity of (3 0 1) plane is dominant for film deposited with 2 M solution concentration attributed to growth mechanism and reorientation effect. Other different weak intensity planes such as (2 1 1), (1 1 0), (1 0 1), (2 0 0) are also observed. The films deposited with 2 M concentration show the highest intensities for (2 1 1) and (3 0 1) plane. It is observed that, by varying the concentration of $SnCl_4$ in spraying solution, the lattice parameter does not get altered. The increase in peak intensity from 0.5 to 2.5 M concentrations may be attributed to the continuous increase in film thickness from 605 to 815 nm. Such type of nature of X-ray diffraction pattern has

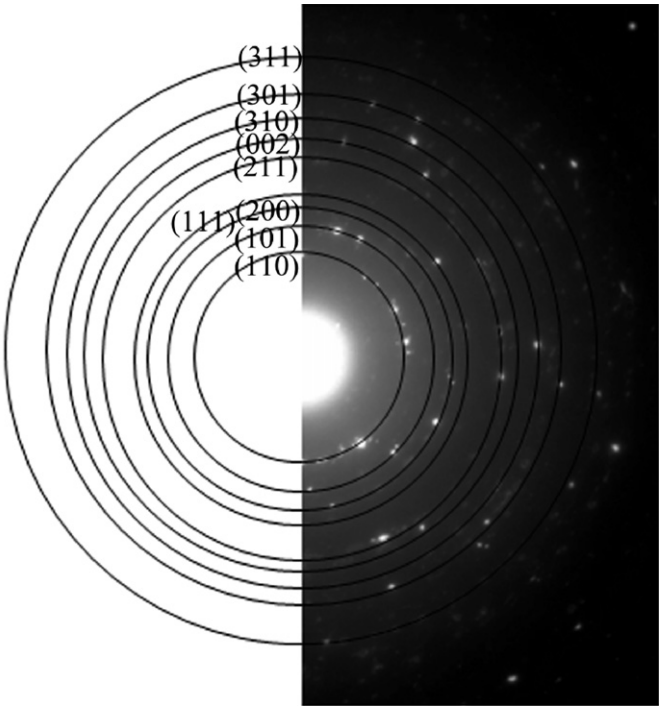

Fig. 3. The selected area electron diffraction (SAED) pattern of typical 2 M concentration.

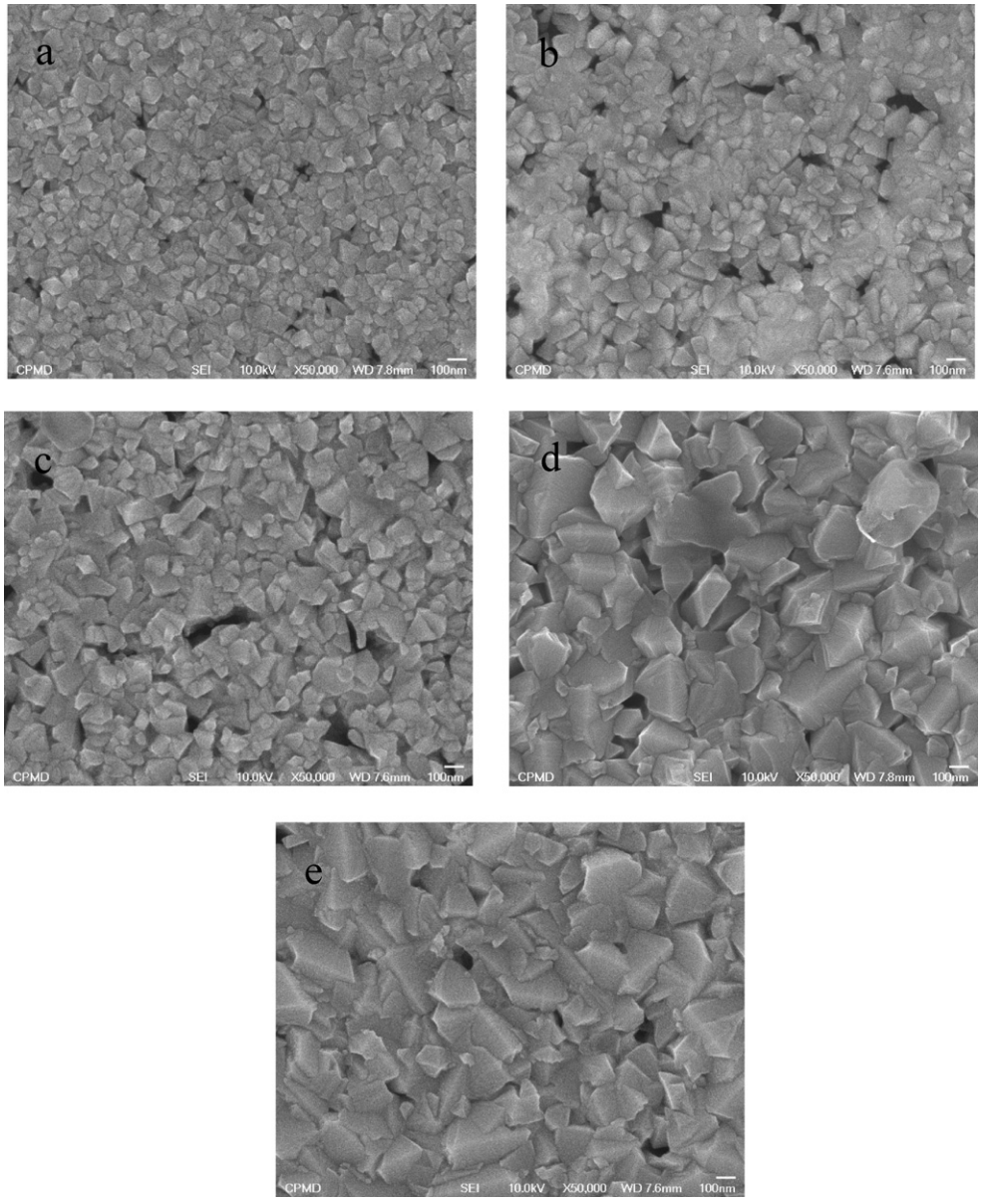

Fig. 4. Field emission scanning electron micrographs of (a) 0.5 M (b) 1 M (c) 1.5 M (d) 2 M and (e) 2.5 M Sb:SnO_2 thin films at various concentrations of $SnCl_4$ in solution.

been observed by Prince et al. [13]. Decrease in (2 1 1) and (3 0 1) peak intensity after 2 M concentration might be due to incomplete thermal decomposition of sprayed droplets because of unsuitable thermal energy (at 475 °C substrate temperature) required for perfect decomposition. For higher concentrations the reorientation effect is probably disturbing the growth, which results in smaller crystallite size. In the present work, no other phases such as SnO and Sn_3O_4 have been observed indicating that the films are of single phase.

The crystallite size '*D*' is calculated using Scherrer's formula,

$$D = \frac{0.9\lambda}{\beta \cos \theta} \quad (1)$$

where *D* is the crystallite size, β is the broadening of the diffraction line measured at half of its maximum intensity (rad.) FWHM and λ is X-ray wavelength (1.5406 Å). The variation of average crystallite size estimated from diffraction line broadening with the solution concentration is shown in Fig. 2. It is found that the crystallite size varies between 12 and 20 nm, increases with the increase in concentration of $SnCl_4$, and reaches a maximum of 20 nm at 2 M and then decreases. The tendency of a decrease in crystallite size with increase in concentration after 2 M may be due to super-saturation of Sn atoms. Similar results have been observed for sprayed FTO thin films. The analysis reveals that the Sn^{4+} ion concentration strongly influences the crystallite size as well as thickness of the thin films. Such effects are common to spray deposited thin films. Fig. 3 shows the selected area electron diffraction (SAED) of typical 2 M concentration Sb:SnO_2 thin film. It shows highly crystalline and well pronounced Scherrer's diffraction rings in the SAED pattern, that can be assigned to the reflections (1 1 0), (1 0 1), (1 1 1), (2 0 0), (2 1 1), (0 0 2), (3 1 0) and (3 1 1) of tetragonal SnO_2. There are no additional rings in the SAED pattern stemming from any crystalline impurities. SAED pattern clearly show deposited films are nanocrystalline and grows along (3 0 1) direction, which is different from common (1 0 1) and (1 1 0) growth direction.

3.2. Morphological study

Fig. 4(a–e) shows the FESEM images of Sb:SnO_2 thin films prepared for various solution molarities ranging from 0.5 to 2.5 M. It

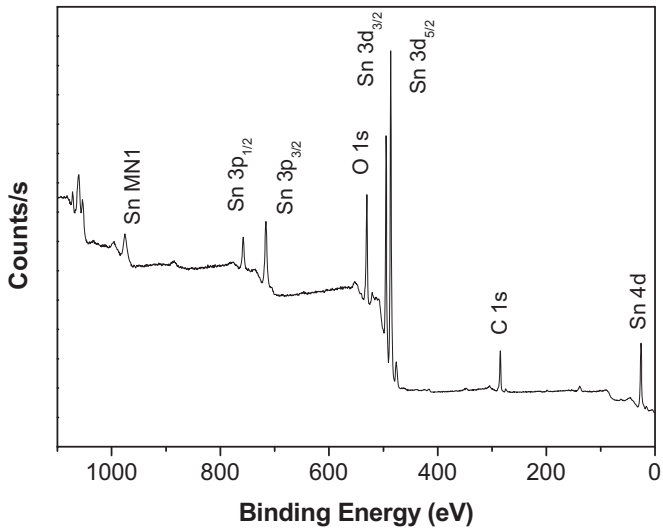

Fig. 5. X-ray photoelectron spectroscopy survey scan spectrum of Sb:SnO_2 thin films at 2 M concentrations of $SnCl_4$ in solution.

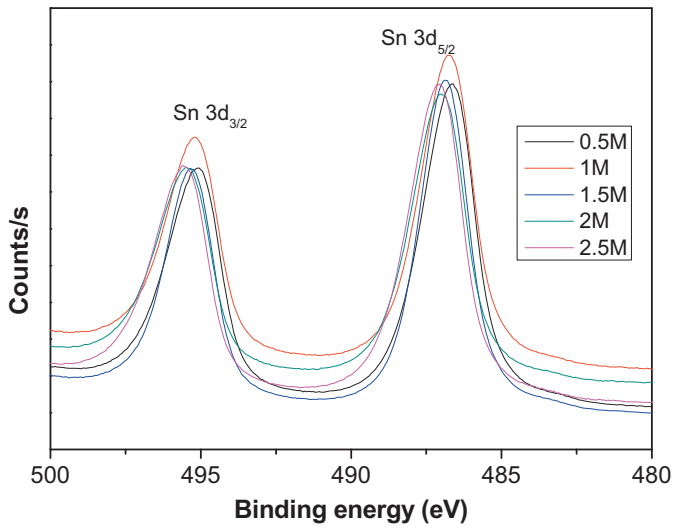

Fig. 6. Sn 3d narrow scan X-ray photoelectron spectroscopy spectra of Sb:SnO_2 thin films deposited at various concentrations of $SnCl_4$ in solution.

was observed that the surface morphology of the films is strongly dependent upon the $SnCl_4$ concentration. At low concentration small polyhedron-like grains are observed. As the $SnCl_4$ concentration increased further, the polyhedron-like grains dwindled and were hardly distinguished from small round grains. The compact and homogenous grains are observed in FESEM images. The grains are randomly grown giving rise to scattering effect thereby reducing transmittance. Some authors discussed the effect of grain size on sensor and optical properties of undoped-SnO_2 [14]. The grain growth is along certain favourable nucleation centres due to which small and large grains are observed. As $SnCl_4$ concentration increases average grain size increases. The average grain size is lies between 100 and 300 nm determined from FESEM study. On the other hand crystallite size for the same samples, as determined from X-ray diffraction analysis is ~12–20 nm, as single aggregate contains number of crystallites. Interestingly, the tendency of high agglomeration among smaller crystallites to form larger agglomerated crystallites was noted for thin film with increased $SnCl_4$ concentration. Moreover the growth rate of the films increases with the solution concentration.

3.3. X-ray photoelectron spectroscopy

Fig. 5 shows the X-ray photoelectron spectroscopy (XPS) survey scan of film deposited with 2 M precursor concentration. Sample contains the Sn, Sb, O and traces of C having Sn MN1 auger peak with Sn 3p, Sn 3d, Sn 4d core levels. The presence of C1s is attributed to contamination which resulted from the samples being exposed to air before the X-ray photoelectron spectroscopic measurements.

Fig. 6 shows the narrow scan XPS spectra of Sn 3d for all samples. The spectra reveals the spin–orbit splitting of the Sn $3d_{5/2}$ ground state to be around 487.1 eV while the Sn $3d_{3/2}$ excited state is observed around 495.4 eV, which is attributed to Sn^{4+} in SnO_2 [15], since $SnCl_4$ was used as precursor. The binding energy of Sn $3d_{5/2}$ is around 487 eV for deposited films which is higher than that of metallic tin (484.65 eV). It confirms that Sn exists only in the oxidized state. The gap between the Sn $3d_{3/2}$ and Sn $3d_{5/2}$ levels (≈8.45 eV) closely correspond to the O in SnO_2 and Sn in SnO_2, respectively. But due to the low doping concentration of Sb, we observe the peak of Sb $3d_{3/2}$ with lower intensity. Terrier et al. [16] reported that the major Sb oxidation states existed as Sb^{5+} state for lower doping level, but as Sb^{3+} state on higher of doping level. They showed that Sb^{5+} peak position was located at 540.1 eV and Sb^{3+} at 539.2 eV of binding energy. In our study, all the samples show the binding energy of Sb $3d_{5/2}$ shown in Fig. 7 is at 530.6–530.9 eV, indicating that all antimony detected was in a pentavalent state (Sb^{5+}). The binding energies of Sb $3d_{5/2}$ are higher than that of metallic Sb (528.3 eV) [17].

Narrow scan XPS spectra of O 1 s for samples deposited with various $SnCl_4$ concentrations (0.5–2.5 M) are shown in Fig. 8(a–e). Generally the O 1s peak has been observed in the BE region of 529–535 eV. The peak around 529–530 eV has been attributed to lattice oxygen. Ghuang and Brundle [18] have attributed the peak around 530.7–531.6 eV to oxygen in non-stoichiometric oxides in the surface region. For chemisorbed O_2 on the metal surface the BE's are found to be in the region 530–530.9 eV, for the surface oxides and hydroxides in the region 529.6–531.0 eV and 533.3 eV, respectively. Sharma et al. [19] have assigned the 532 eV peak to absorbed hydroxyl ions. On the basis of the above, the O 1s peak observed in the region 530.47–530.87 eV for Sb:SnO_2 thin film prepared by spray pyrolysis in the present work can be attributed to chemisorbed oxygen. The peak appeared around 532 eV attributed to the OH group linked to Sn. This has been observed for all samples, indicating samples are hygroscopic in nature. Carbon atoms in

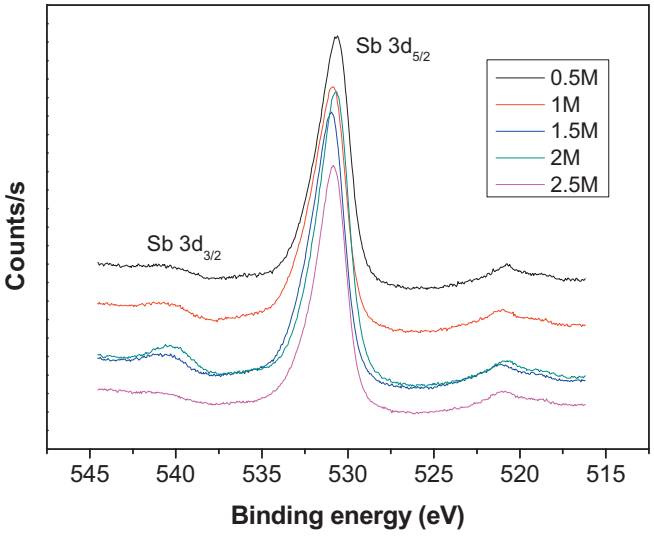

Fig. 7. Sb 3d narrow scan X-ray photoelectron spectroscopy spectra of Sb:SnO_2 thin films deposited at various concentrations of $SnCl_4$ in solution.

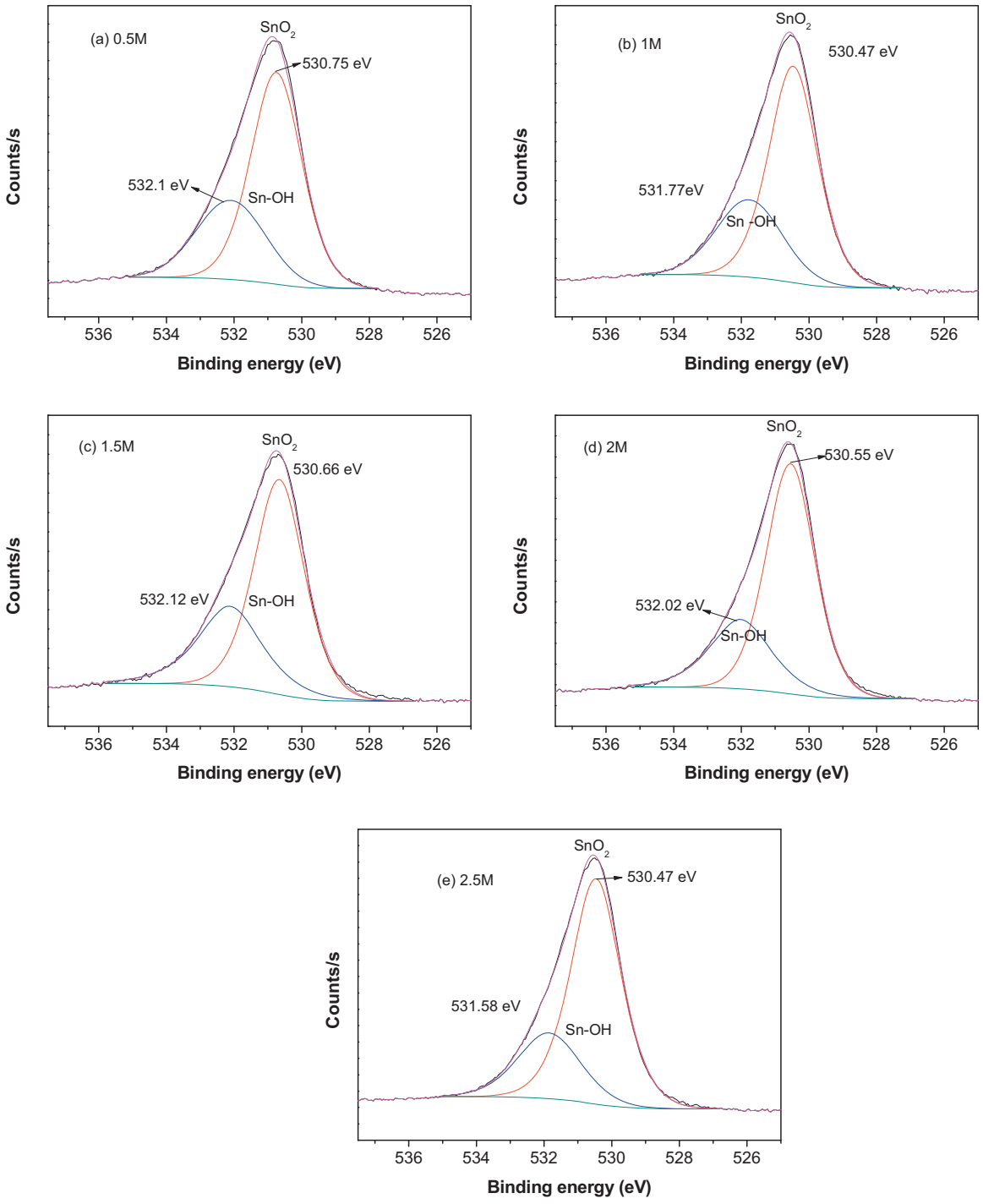

Fig. 8. O 1s narrow scan X-ray photoelectron spectroscopy spectra of Sb:SnO_2 thin films deposited at various concentrations of $SnCl_4$ in solution; (a) 0.5 M, (b) 1 M, (c) 1.5 M (d) 2 M and (e) 2.5 M.

three position from a carboxyl group (C–C, 285 eV,), (C–O, 286 eV) and (C=O, 288 eV) respectively. The ratio of atomic concentrations (O/Sn) is quantitatively analyzed by calculating the peak areas of O 1s and Sn $3d_{5/2}$ peaks. The values are deviated from theoretical one, which confirms the sample deposited with 2 M $SnCl_4$ solution concentration is oxygen deficient.

3.4. Optical properties

Information concerning optical transmittance found to be very important for evaluating optical performance of conducting oxide films. A high transparency in visible region for tin oxide thin films is required for optoelectronic devices. Fig. 9 shows the wavelength dependence on optical transmittance of Sb:SnO_2 thin films deposited on glass substrates with various $SnCl_4$ concentrations. At lower concentration Sn goes only at regular sites results into maximum transmittance. When Sn concentration exceeds a limit gradual occupation of interstitial of tin may take place and this phenomenon changes the preferred growth of the films. Due to this films with some defects may results into decrease in transmittance. The visible and near-IR regions are the transparent region for the films. The transmission in this region is limited by sev-

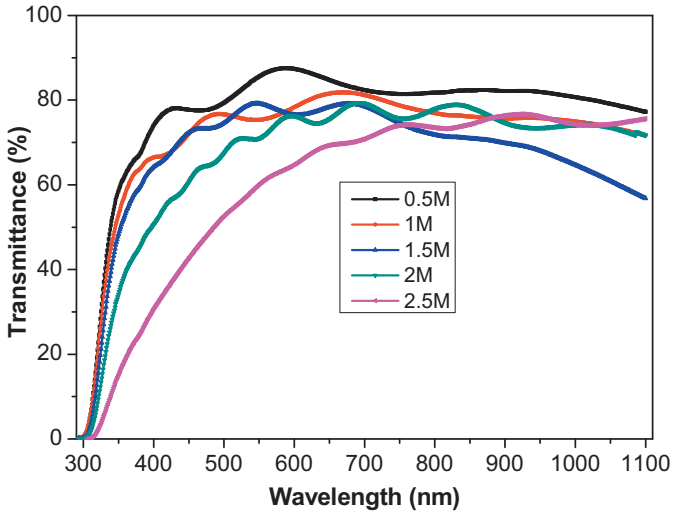

Fig. 9. Variation of transmittance with discrete wavelengths for the sprayed Sb:SnO_2 thin film deposited at different concentrations of $SnCl_4$ in solution.

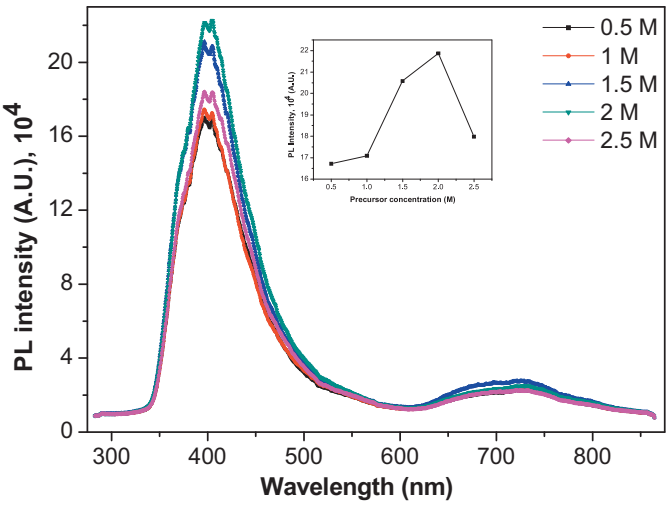

Fig. 10. Photoluminescence emission spectra of Sb:SnO_2 thin films with different $SnCl_4$ concentrations in solution (the inset shows the plots of photoluminescence intensity versus $SnCl_4$ concentration).

eral factors: (1) reflection losses which include both specular and scattered (diffuse) components (this backward scattering (about 1–2%) is primarily due to surface roughness and increases with increasing thickness); (2) absorption (about 1–2%) [20] in the film, which is primarily due to free carriers; (3) variations in transmittance that, depending on the thickness of the film, may occur due to interference phenomena with the result that an average visible transmission must be described. The transmitted part of the incident energy also has specular and scattered (diffuse) components. This forward scattering (about 5%) is due to inhomogeneities in the film in the form of unreacted or partly reacted chemical species generated during the complex pyrolytic process, trapped gases, segregated impurity atoms or other oxide phases. The well-developed interference patterns in T show that the films are specular to the great extent. Furthermore, there is a shift in the absorption edge to shorter wavelength with increasing $SnCl_4$ concentration which is due to the Burstein–Moss shift [21]. Thin films often show a small band gap widening and the absorption edge moves to a shorter wavelength than that of the bulk material.

It is seen that the direct optical band gap (E_g) has decreased from 3.60 eV to 3.50 eV with $SnCl_4$ concentration. The band gap energy determined in this way is not the actual band gap of the deposit as these are degenerate semiconductors, the Fermi level lies within the conduction band where its position depends on the density of the free electrons. Thus, the values given for the optical band gaps are related to the excitation of the electrons from the valance band to the Fermi level in the conduction band, whereas the actual band gap of the material is related to the excitation of the electrons from the top of the valence band to the bottom of the conduction band. This means that the lifting of the Fermi level into the conduction band of the degenerate semiconductor due to the increase in the carrier density leads to the energy band broadening (shifting). However, when SnO_2 is doped with antimony and the carrier concentration is of the order of 10^{20} cm^{-3}, a substantial band gap widening is expected. Similar results have been obtained for spray deposited SnO_x, SnO_x:F, and SnO_x:Sb films [22].

3.5. Photoluminescence

The room temperature photoluminescence spectra of the Sb:SnO_2 thin films prepared with different $SnCl_4$ concentrations were recorded in the range 530–850 nm is shown in Fig. 10. Deep level emission in the visible spectrum is generally attributed to native defects. Point defects such as oxygen vacancies and complexes involving tin interstitials, tin and oxygen vacancies are known to contribute to visible emission. For all the samples an intensive violet emission peak is observed in the region 393–395 nm (3.15–3.13 eV) and shoulders around 366 nm (3.38 eV), 422 nm (2.93 eV) and 474 nm (2.61 eV) are observed. The inset shows the photoluminescence intensity brightness (violet peak) against solution concentration. With increase in solution concentration, the intensity of violet peak increases and attains maximum value at 2 M concentration due to non-radiative recombination [23]. Kim et al. [24] reported peak at 3.1 eV for undoped SnO_2 observed in low temperature and room temperature, and they thought that the origin of the peak was related to oxygen vacancies. The high density of oxygen vacancies interact with interfacial tin leads to the formation of a considerable amount of trapped states within the band gap giving rise to high photoluminescence intensity at room temperature. For our samples, because of the pyrolytic decomposition, there should be existence of oxygen vacancies due to rapid evaporation and oxidation process. The origin of peak in the region 393–395 nm (3.15–3.13 eV) is attributed to the electron transition from donor level formed by oxygen vacancies (V_O) or Sb^{5+} ions to the acceptor level formed by Sb^{3+} ions [24]. The basis of peak at 422 nm (2.93 eV) can be ascribed to the luminescence centres formed by tin interstitials (Sn_i) or dangling bonds present in the SnO_2 thin films [25]. Other peak appeared at 474 nm (2.61 eV), which corresponds to blue luminescence and can be attributed to singly charged oxygen vacancies (V_O) in the films. [26]. The orange emission observed in the region 661–665 nm might be due to involvement of an interstitial oxygen (O_i) ions [27]. Broad peak observed in the region 715–720 nm for all films may be due to other crystal defects which are formed during the growth of samples. It is seen that, there is slight shifting in emission lines due to Sn_i, O_i and V_O dominate in the defect structure of Sb:SnO_2 due to the multivalence of tin, explaining the natural non-stoichiometry of this material [28]. At low concentration, crystallization of the film is poor, due to generation of large number of defects in the films, which can lead to non-radiative recombination and weaken the intensity of the violet emission. When concentration increases, X-ray diffraction pattern (Fig. 1) and FESEM images (Fig. 4) show that the samples have better crystallization, which means that the number of defects in the films and the non-radiative recombination decreases accordingly. In addition, better crystallization makes the substitution doping of Sb more ideal and the donor level formed

by Sb ions is enhanced, so the intensity of the violet peak increases with the increase of $SnCl_4$ concentration. In SnO_2, the Sn 4d electron interacts strongly with the O 2p electron. The emission peaks around 366 nm (3.38 eV), 422 nm (2.93 eV) and 474 nm (2.61 eV) are smaller than the band gap of 3.62 eV of SnO_2, and so these visible emission peaks cannot be ascribed to the direct recombination of a conduction electron in the Sn 4d band and a hole in the O 2p valence band. The position of the violet peak shows slight blue shift with increase in solution concentration due to donor level formed by Sb ions and oxygen vacancies.

3.6. Gas sensing properties

3.6.1. Effect of operating temperature on to response of Sb:SnO_2 films

Fig. 11 shows the response as a function of operating temperature for Sb:SnO_2 films obtained for different concentrations. It is seen that, gas response increases with operating temperature up to 450 °C and then decreases for higher temperatures. The response of all the films does not exhibit any significant difference at lower temperatures. At a low operation temperature, the low response can be expected due to the gas molecules do not have enough thermal energy to react with the surface adsorbed oxygen species. The electrons are drawn from the conduction band of the Sb:SnO_2 by the adsorbed oxygen, and a potential barrier to charge transport is developed. At higher temperatures the thermal energy obtained was high enough to overcome the potential barrier, and a significant increase in electron concentration resulted from the sensing reaction. The response of a semiconductor oxide gas sensor to the presence of a given gas depends on the speed of the chemical reaction on the surface of the grains and the speed of diffusion of the gas molecules to that surface which are activation processes, and the activation energy of the chemical reaction is higher. In this case,

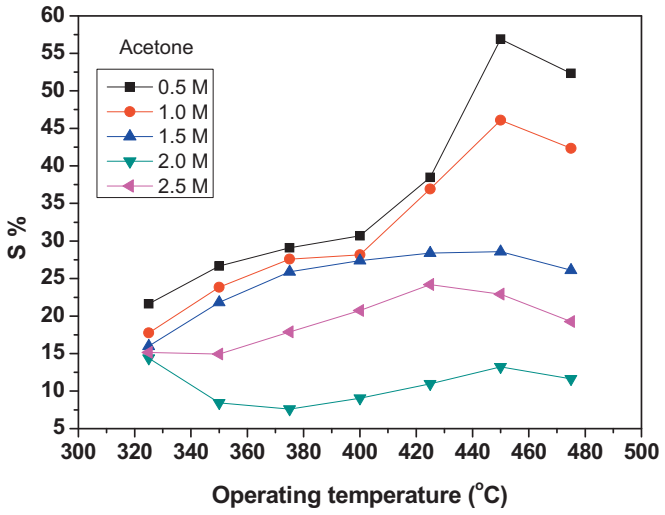

Fig. 11. Gas responses as a function of operating temperature for acetone.

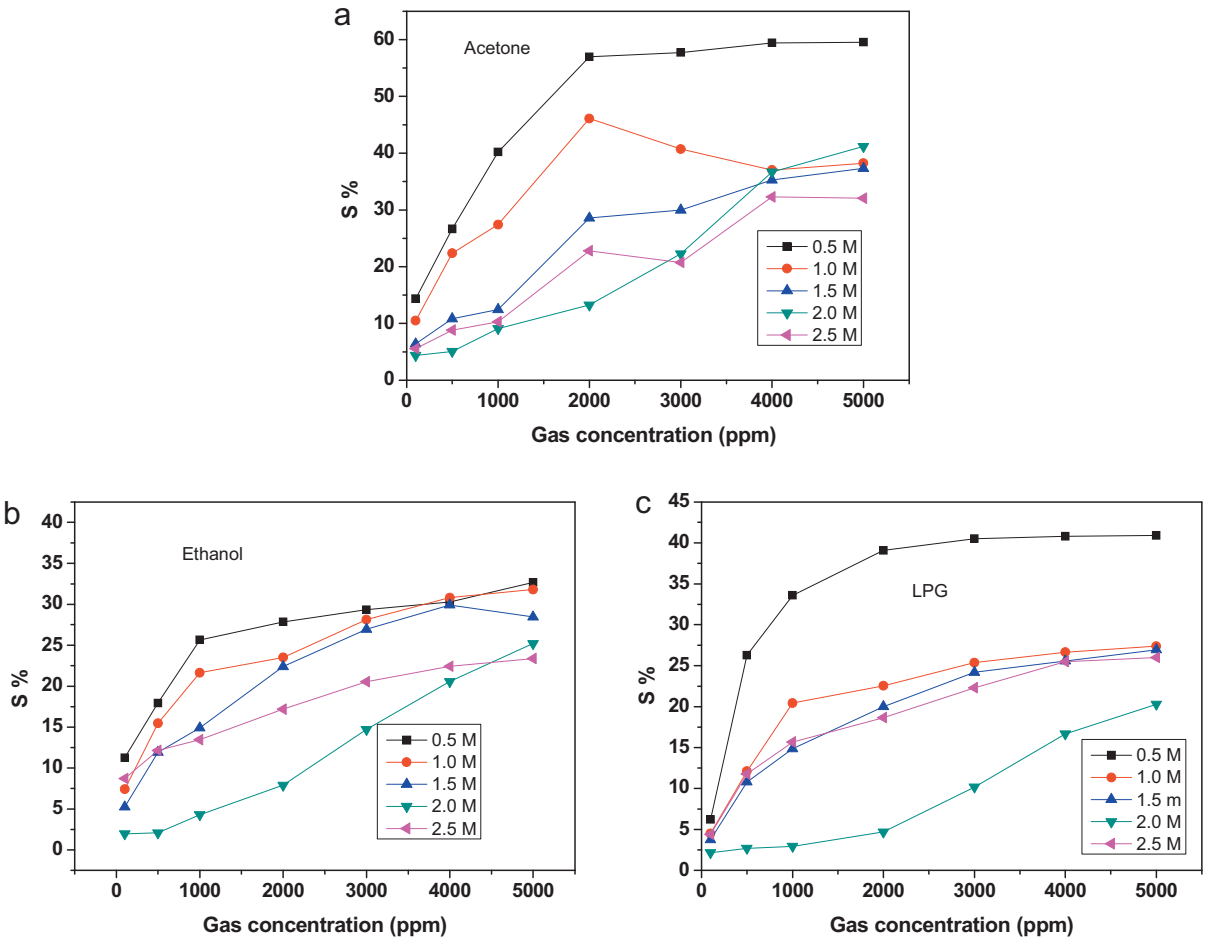

Fig. 12. Variation in gas response of the Sb:SnO_2 films with (a) acetone, (b) ethanol and (c) LPG gas concentration respectively at 450 °C.

at low temperatures the sensor response is restricted by the speed of the chemical reaction, and at higher temperatures it is restricted by the speed of diffusion of gas molecules. At some intermediate temperature, the speed values of the two processes become equal, and at that point the sensor response reaches its maximum [29]. Thus, in the present case the optimum operating temperature for Sb:SnO_2 films was 450 °C at which the Sb:SnO_2 sensor response attained its peak value. The temperature, which corresponds to a certain peak value, is a function of target gases, the chemical composition of the oxide, including additives and catalysts, and pure oxides are generally stable at lower temperatures. So the high operating temperature is necessary for Sb:SnO_2 films to interact with the acetone, ethanol and LPG gas.

Furthermore, it can be evidenced from the figure that for 0.5 M, the response was maximum (56%) at 450 °C, and it was larger than those of other films. It is well known that the gas response of the metal-oxide semiconductor sensors is mainly determined by the interactions between a target gas and the surface of the sensors. So it is obvious that for the greater surface area of the materials, the interaction between the adsorbed gases and the sensor surface are stronger, i.e., the gas response is higher [30]. In the present case, it has been seen from SEM images show more surface area to interact gas molecules at 0.5 M concentration, whereas the dense and bigger grains are observed for greater concentrations. The total surface area and grain boundary are largest for 0.5 M. With the largest number of adsorption–desorption sites, the response could be improved by the significant change in surface area.

3.6.2. Effect of gas concentration on the response of Sb:SnO_2 films

Fig. 12(a–c) shows the response of films as a function of various gases concentration at 450 °C. As concentration increases the sensitivity increases with gas concentration from 15 to 57%, 10–28% and 6–40% for acetone, ethanol and LPG gases respectively. The figure reveals that the gas response increases up to 2000 ppm concentration and then saturates for higher gas concentration. However, at higher concentrations the increase in gas response value was gradual and the response saturated for all gas concentrations more than 2000 ppm. The response of a sensor depends on removal of adsorbed oxygen molecules by reaction with a target gas and generation of electrons. For a small concentration of gas, exposed on a fixed surface area of a sample, there is a lower coverage of gas molecules on the surface and hence lower surface reaction occurred. An increase in gas concentration increases the surface reaction due to a larger surface coverage. A further increase in surface reaction will be gradual when the saturation point on the coverage of molecules is reached. Further it was seen that almost the same time is taken to reach the maximum response for different concentrations of gases and the response dropped rapidly when the gas is removed from the testing atmosphere, indicating that the sensor had good response and recovery characteristics at higher concentrations of the gas. Thus, maximum response of 57, 28 and 40% is obtained at 450 °C upon exposure to 2000 ppm of gas for acetone, ethanol and LPG respectively.

3.6.3. Conclusions

The effect of the molar concentration on the gas sensing characteristics of Sb:SnO_2 films prepared by spray pyrolysis was studied. The films are polycrystalline with tetragonal crystal structure showing crystal reorientation effect as well as enhancement in grain size confirmed from FESEM and SAED. The direct optical band gap (E_g) has decreased from 3.60 to 3.50 eV with increase in $SnCl_4$ concentration. Oxygen vacancies or donor level formed by Sb ions are the dominant luminescent centres for the emission of violet light in SnO_2 thin films. The spray deposited Sb:SnO_2 films were sensitive to acetone, ethanol and LPG with 57, 28, 40% response at 2000 ppm concentration respectively.

Acknowledgement

One of the authors (A.R. Babar) is highly grateful to University Grants Commission, New Delhi for its support through UGC meritorious fellowship.

References

[1] J.I. Yang, H. Lim, S.D. Han, Sens. Actuat. B 60 (1999) 71–77.
[2] G. Jiménez-Cadena, J. Riu, F.X. Rius, Analyst 132 (2007) 1083–1099.
[3] M. Siemons, A. Leifert, U. Simon, Adv. Funct. Mater. 17 (2007) 2189–2197.
[4] J. Rockenberger, U. Zum Felde, M. Tisher, L. Troger, M. Hasse, H. Weller, J. Chem. Phys. 112 (2000) 4296–4304.
[5] A.R. Babar, S.S. Shinde, A.V. Moholkar, C.H. Bhosale, J.H. Kim, K.Y. Rajpure, J. Alloy Compd. 505 (2010) 416–422.
[6] S.S. Shinde, P.S. Patil, R.S. Mane, B.N. Pawar, K.Y. Rajpure, J. Alloy Compd. 503 (2010) 416–421.
[7] G. Shanon, R. Rup, A. Manansingh, Thin Solid Films 190 (1989) 287–301.
[8] J.L. Huang, Y. Pan, J.Y. Chang, B.S. Yau, Surf. Coat. Technol. 184 (2004) 188–193.
[9] G. Gasparro, J. Putz, D. Ganz, M.A. Aegerter, Sol. Energy Mater. Sol. Cell 54 (1998) 287–296.
[10] H. Viirola, L. Niinistö, Thin Solid Films 251 (1994) 127–135.
[11] G. Jain, R. Kumar, Opt. Mater. 26 (2004) 27–31.
[12] A.L. Unaogu, C.E. Okeke, Solar Energy Mater. 20 (1990) 29–36.
[13] J.J. Prince, S. Ramamurthy, B. Subramanian, C. Sanjeeviraja, M. Jayachandran, J. Cryst. Growth 240 (2002) 142–151.
[14] M. Losurdo, D. Barreca, P. Capezutto, G. Bruno, E. Tondello, Surf. Coat. Technol. 151 (2002) 2–8.
[15] D. Kim, S. Kim, Surf. Coat. Technol. 176 (2003) 23–29.
[16] C. Terrier, J.P. Chatelon, J.A. Roger, J. Sol–Gel Sci. Technol. 10 (1997) 75–81.
[17] J. Kong, H. Deng, P. Yanga, J. Chua, Mater. Chem. Phys. 114 (2009) 854–859.
[18] T.J. Ghuang, C.R. Brundle, D.W. Rice, Surf. Sci. 59 (1976) 413–429.
[19] D.D. Sharma, M.S. Hegde, C.N.R. Rao, J. Chem. Soc. Faraday Trans. II 77 (1981) 1509.
[20] K.L. Chopra, S. Major, D.K. Pandya, Thin Solid Films 102 (1983) 1–46.
[21] M. Girtan, G.I. Rusu, S. Gurlui, Appl. Surf. Sci. 162 (2000) 492–498.
[22] E. Shanti, A. Banerjee, L.K. Chopra, Thin Solid Films 88 (1982) 93–100.
[23] Y. Wang, J. Ma, F. Ji, X. Yu, H. Ma, J. Luminescence 114 (2005) 71–76.
[24] T.W. Kim, D.U. Lee, Y.S. Yoon, J. Appl. Phys. 88 (2000) 3759–3761.
[25] D. Calestani, L. Lazzarini, G. Salviati, M. Zha, Cryst. Res. Technol. 40 (2005) 937–941.
[26] S. Rani, S.C. Roy, N. Karar, M.C. Bhatnagar, Solid State Commun. 141 (2007) 214–218.
[27] D. Zhang, D. Guo, X. Pu, X. Shao, R. Liu, L. Li, X. Qian, Mater. Lett. 63 (2009) 2290–2293.
[28] Ç. Kiliç, A. Zunger, Phys. Rev. Lett. 88 (2002) 095501.
[29] T.G. Nenov, S.P. Yordanov, Ceramic Sensors, Technology and Applications, Technomic Publishers, Lancaster, 1996, p. 138.
[30] J.F. Chang, H.H. Kuo, I.C. Leu, M.H. Hon, Sens. Actuat. B 84 (2002) 258–264.